www.czasopisma.pan.pl PAN POLSKA AKADEMIA NAUK www.journals.pan.pl

Arch. Metall. Mater. **69** (2024), 1, 189-196

DOI: https://doi.org/10.24425/amm.2024.147808

HAO LIN[1*], HAIPENG GENG[2], XIFENG ZHOU[2], LEIMING SONG[1], XIAOJUN HU[1]

INVESTIGATION ON MECHANICAL PROPERTIES OF MAR-M247 SUPERALLOY FOR TURBINE BLADES BY EXPERIMENT AND SIMULATION

This study aimed to investigate the metallographic structure and the impact of the heat treatment process on the MAR-M247 superalloy, a high-temperature nickel-based superalloy commonly used in turbine blades. The heat treatment process can potentially influence the mechanical properties of the MAR-M247 superalloy at different temperatures. A strength simulation analysis of gas turbine blades should include the variations in the mechanical properties of the material. The effect of heat treatment on grain size was investigated by metallographic experiments, and numerical calculations of material mechanical properties were conducted. The mechanical property parameters necessary for finite element analysis of turbine blades were determined. Finally, a finite element simulation model of the blade was established based on these mechanical property parameters, and strength analysis was performed. The simulation results provided the stress distribution and the strength of the turbine blade.

Keywords: Heat treatment; MAR-M247 nickel-based superalloy; mechanical properties; strength analysis; turbine blade

1. Introduction

Turbine blades bear the centrifugal load, thermal load, aerodynamic load, vibration load, and corrosion from high-temperature gas during operation. Despite advancements in cooling and coating technology, the strength requirements for turbine blades remain crucial. First, the blade materials should have good yield strength, tensile strength, and creep strength to meet deformation and accuracy requirements. Second, the materials should have sufficient creep strength to withstand temperature demands [1]. Third, the material should have high-cycle and low-cycle fatigue strengths [2].

Based on the aforementioned strength requirements, the materials currently used in turbine blades are generally high-temperature superalloys. High-temperature superalloys are alloys of iron, cobalt, or nickel. They are oxidation or corrosion resistant at high temperatures (more than 600°C) and maintain structural integrity for a long time under certain stress conditions [3]. The high-temperature nickel-based superalloys are well-suited for turbine blades. These superalloys are based on nickel and are solid-solution strengthened with various alloy elements. They exhibit good structural stability. The strengthening phase is achieved through the formation of a coherent A_3B-type intermetallic compound, known as phase γ'. Nickel-based superalloys have better mechanical properties than iron- and cobalt-based alloys at high temperatures (more than 760°C) [4].

To date, high-temperature superalloys have been the most widely used materials in turbine blades. The MAR-M247 superalloy is the first generation of directionally solidified superalloys. Its chemical composition (in wt.%) is outlined in TABLE 1.

TABLE 1

Chemical composition of MAR-M247 superalloy (in wt.%)

C	Cr	Mo	Al	Co	Ti	Fe	W	Hf	B	Ta	Zr	Ni
0.16	8.6	0.8	5.6	10.0	1.0	0.2	10.0	1.5	0.02	3.0	0.06	Rest

The equiaxed crystal structure of the MAR-M247 superalloy has excellent mechanical properties at high temperatures. The MAR-M247 superalloy has replaced Inconel 713LC alloy and is currently widely used in blade disks with operating temperatures of 1000°C [5]. The MAR-M247 superalloy is being increasingly used in gas turbine blades [6]. This study aimed to focus on the MAR-M247 superalloy.

When different heat treatment processes were applied to the MAR-M247 superalloy, different sizes of metal lattices and

[1] SCHOOL OF MECHANICAL, ELECTRONIC AND CONTROL ENGINEERING, BEIJING JIAOTONG UNIVERSITY, BEIJING, 100044, P.R. CHINA
[2] SCHOOL OF MECHANICAL ENGINEERING, XI'AN JIAOTONG UNIVERSITY, XI'AN, 710049, P.R. CHINA

* Corresponding author email: haol@bjtu.edu.cn

© 2024. The Author(s). This is an open-access article distributed under the terms of the Creative Commons Attribution-NonCommercial License (CC BY-NC 4.0, https://creativecommons.org/licenses/by-nc/4.0/deed.en which permits the use, redistribution of the material in any medium or format, transforming and building upon the material, provided that the article is properly cited, the use is noncommercial, and no modifications or adaptations are made.

grains were obtained. The mechanical properties of the material also changed. The multistep solid solution treatment for the MAR-M247 superalloy increased the initial temperature of the heat treatment. The primary phase γ' transformed into the secondary phase γ' and the 90% dissolved eutectic phase γ/γ' [7]. The multistep aging treatment achieved better mechanical properties of phase γ'. Meanwhile, its tensile strength and fracture life also improved [8].

Some studies investigated the directionally solidified superalloy and found that the microstructure was incomplete solid solution after the solid solution treatment at 1210°C. When the solid solution temperature was 1260°C, a small amount of melting occurred in the microstructure. The heat treatment process influenced the mechanical properties, and good comprehensive mechanical properties could be obtained through a specific heat treatment. In this paper, the heat treatment process is determined to be: 1230°C/2 h/ air cooling +980°C/5 h/ air cooling +870°C/20 h/ air cooling [9].

Metallographic experiments showed that the heat treatment impacted the grain size. The mechanical properties of the MAR-M247 superalloy were also changed by the heat treatment process. Some studies carried out numerical calculations and finite element analysis on the strength of gas turbine blades [10-13]. However, the strength simulation analysis of gas turbine blades mostly does not consider the effect on the mechanical properties of the material used. Hence, the effect of heat treatment on improving material mechanical properties is not considered. Therefore, we aimed to accurately obtain the mechanical property parameters of the MAR-M247 superalloy to analyze the strength of the turbine blade.

This study first focused on the metallographic structure and effect of the heat treatment on the MAR-M247 superalloy. Metallographic experiments were performed to examine the impact of heat treatment on the grain size, and numerical calculations of mechanical properties were carried out. The mechanical property parameters were obtained for the strength analysis of turbine blades. Finally, the finite element simulation model of the turbine blades was established, and the strength analysis was carried out.

2. Heat treatment experiment and metallographic analysis

In this study, the MAR-M247 superalloy was fabricated by directional solidification. The hexahedron samples (length × width × height = 5 × 5 × 10 mm^3) were subjected to heat treatment in the WZ-30 vacuum furnace. The heat treatment process was set as 1230°C/2 h/ air cooling +980°C/5 h/ air cooling +870°C/20 h/ air cooling [14].

After heat treatment, the sample was polished using silicon carbide sandpaper on a metallographic polishing machine. The scanning electron microscope (SEM) and the energy dispersive spectrometer (EDS) were used to analyze the samples. The instruments used was JSM-6390AT. The surface morphology was analyzed, and composition and proportions were determined. Samples without heat treatment were also analyzed and compared.

The results of the metallographic analysis for the MAR-M247 superalloy without heat treatment are depicted in Fig. 1.

The results of the metallographic analysis for the MAR-M247 superalloy with heat treatment are depicted in Fig. 2.

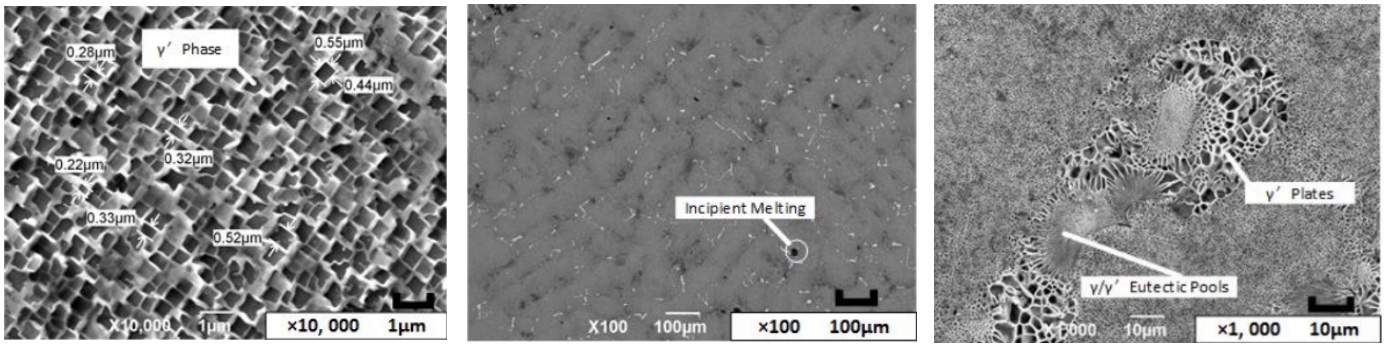

Fig. 1. Results of metallographic analysis for MAR-M247 superalloy (without heat treatment)

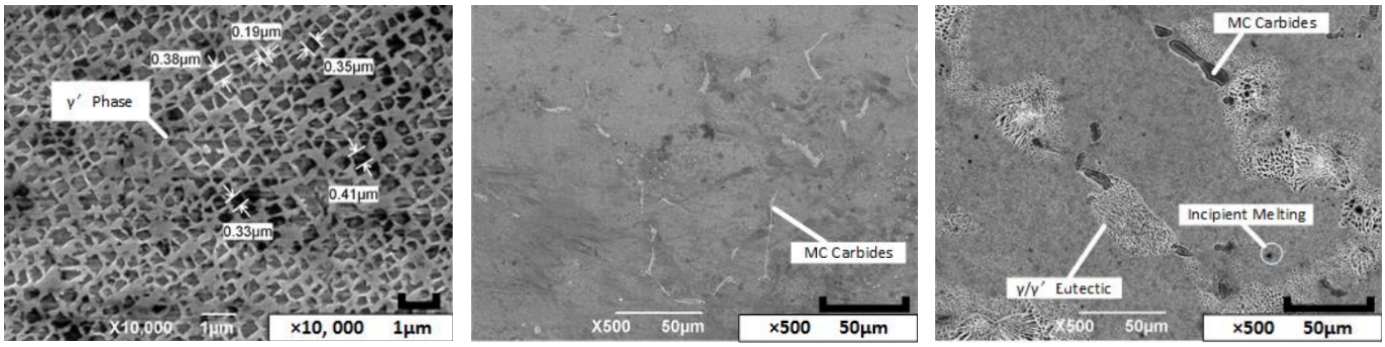

Fig. 2. Results of metallographic analysis for MAR-M247 superalloy (with heat treatment)

The grain sizes and distribution were obtained at a magnification of 10,000 through a metallographic experiment, and the surveyor's rod was 1 μm. The grain sizes of the MAR-M247 superalloy without heat treatment were relatively large (0.28-0.55 μm) (Fig. 1). The grain sizes of the MAR-M247 superalloy after the heat treatment were refined (0.19-0.38 μm), and the shapes of grains were mostly quadrilateral (Fig. 2). The grain sizes with heat treatment were smaller. The number of dislocations was increased compared with those without heat treatment.

The grain sizes were calculated following the average method. The grain size of the phase γ' without heat treatment was about 0.45 μm, and that with heat treatment was approximately 0.3 μm. This indicated that the grains of the MAR-M247 superalloy without heat treatment were coarser than those after heat treatment.

Fig. 1 shows the distribution of different phases without heat treatment. The distribution of carbides (MC) could be clearly observed with incipient melting. The figure also shows elongated carbides and the distribution of the eutectic phase γ/γ' without heat treatment. However, the long carbides were distributed discretely after heat treatment, as shown in Fig. 2. The distribution of carbides, eutectic phase γ/γ', and incipient melting became uniform. Comparing Fig. 2 with Fig. 1, the size of the eutectic phase γ/γ' was smaller after heat treatment.

Fig. 3 shows the material composition results of the MAR-M247 superalloy after heat treatment as analyzed using EDS.

Fig. 4 shows the EDS results of the carbide defect without heat treatment.

Fig. 5 shows the EDS results of the carbide defect after heat treatment.

Fig. 4 and Fig. 5 show that the carbides were TaC, WC, TiC and HfC. The amount of each component at different positions was also different.

Comparing Fig. 5 and Fig. 3, it could be concluded that the content of TaC was the highest in carbides, accounting for half of the content on average. The smaller the size of the carbide, the lower the content of TaC and WC, and the higher the content of TiC and HfC.

The metallographic results were analyzed using the aforementioned experiments. The heat treatment process was found to have an influence on the phase γ', carbides, and the eutectic phase γ/γ'. The mechanical properties of the MAR-M247 superalloy were obtained as described in the following Section 3.

3. Numerical calculation of material properties

The standard round rod specimens of the MAR-M247 superalloy were used in the experiment. The heat treatment process for the round rod specimens was the same as: 1230°C/2 h/ air cooling +980°C/5 h/ air cooling +870°C/20 h/ air cooling. The tensile tests were conducted on a tensile testing machine. The results are presented in TABLE 2.

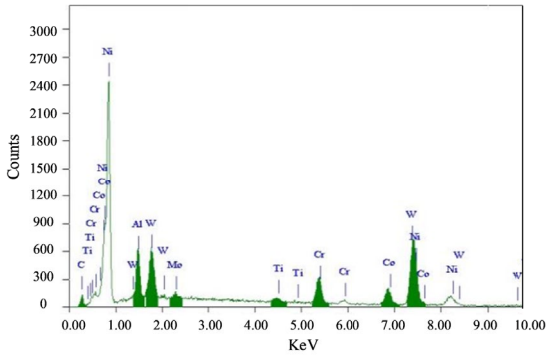

Fig. 3. Compositional results of the MAR-M247 superalloy analyzed using EDS

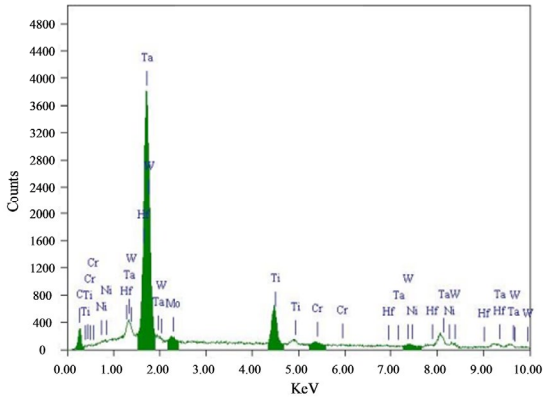

Fig. 4. EDS results of the component in the carbide defect (without heat treatment)

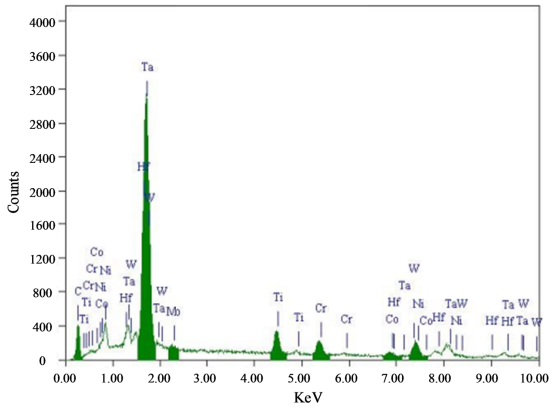

Fig. 5. EDS results of the component in the carbide defect (with heat treatment)

TABLE 2

Tensile test results of MAR-M247 specimens

Temperature (°C)	$\sigma_{0.2}$ (MPa)	σ_m (MPa)	Elongation (%)	Shrinkage (%)
20	876	937	5.7	6.7
900	640	724	7.3	10.0

Numerical calculations were conducted using material property simulation software. The numerical simulation results are illustrated in Figs. 6-8.

Fig. 6 shows the results of the yield strength. The yield strength at 800°C was calculated to be 740 MPa, which decreased significantly compared with the yield strength at room temperature.

Fig. 7 shows the stress-strain relationship of the MAR-M247 superalloy. After exceeding the yield strength limit of the material, the stress value remained more than 800 MPa.

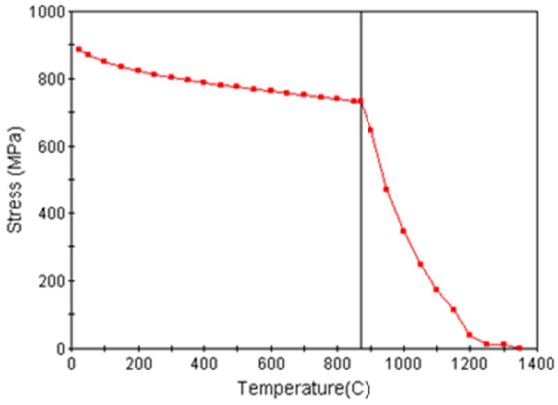

Fig. 6. Relationship between yield strength and temperature

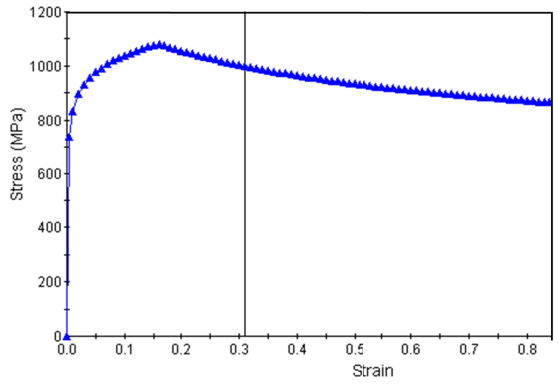

Fig. 7. Relationship between Stress and strain at 800°C

As depicted in Fig. 8, the tensile strength of the material at 800°C was 885 MPa.

Fig. 9 shows the relationship between temperature and Young's modulus.

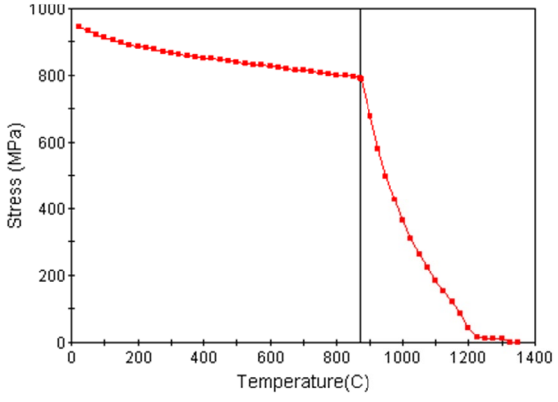

Fig. 8. Relationship between tensile strength and temperature

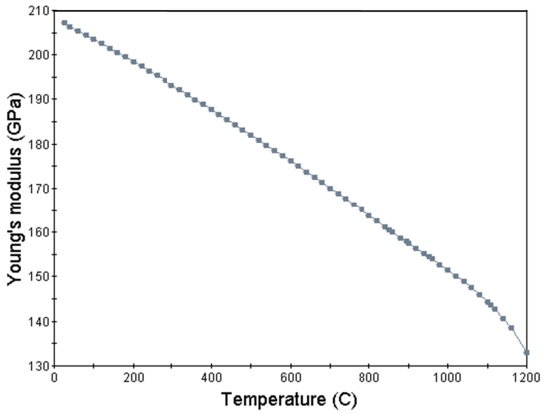

Fig. 9. Relationship between temperature and Young's modulus

Figs. 10 and 11 show the relationship between the coefficient of thermal expansion and temperature and between temperature and thermal conductivity, respectively.

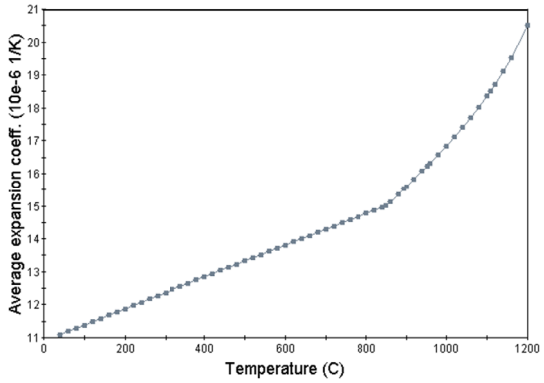

Fig. 10. Relationship between coefficient of thermal expansion and temperature

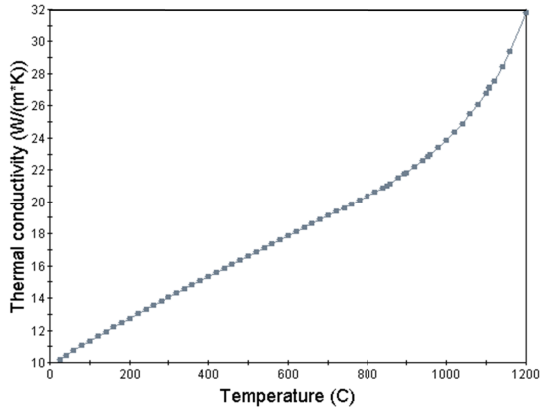

Fig. 11. Relationship between thermal conductivity and temperature

The numerical calculation results are presented in TABLE 3, providing mechanical property parameters for strength simulation analysis of turbine blades.

The experimental findings of $\sigma_{0.2}$ at 900°C could verify the numerical calculation, affirming the reliability and effectiveness of the results.

TABLE 3

Mechanical properties of the MAR-M247 superalloy

Temperature (°C)	20	400	500	600	700	800	900
Young's modulus (GPa)	207	189	184	177	170	166	158
Yield strength (MPa)	877	789	775	763	751	740	640
Tensile strength (MPa)	936	901	894	886	880	848	725
Coefficient of thermal expansion (10^{-6}/K)	—	12.92	13.41	13.87	14.34	14.82	15.55
Thermal conductivity (W/m*K)	10.24	15.47	16.76	18.02	19.26	20.52	21.94

The mechanical properties of the MAR-M247 superalloy were calculated based on the tensile test data. The results provided crucial mechanical property parameters for the strength simulation analysis of turbine blades.

3. Finite element analysis

In actual operating conditions, heavy-duty gas turbine blades, as shown in Fig. 12, operate in environments characterized by high temperature, high load, and prolong exposure to corrosion. The loads acting on blades mainly include centrifugal stress, thermal stress, and airflow excitation force. The mechanical property parameters of the MAR-M247 superalloy could accurately calculate the maximum stress of turbine blades [15]. This is crucial in evaluating their strength.

The finite element modeling of the blade was constructed using tetrahedral mesh elements (with an element size of 1 mm), as shown in Fig. 13. A total of 1,204,283 elements and 1,809,976 nodes were included.

The finite element simulation analysis of the blade was conducted, and the stress distribution of the blade is shown in Fig. 14.

Fig. 14 shows that stress concentration positions were located at the tenon teeth and round corners near the listrium in the suction surface and the pressure surface. The stress distribution in the middle of the blade was relatively uniform. The stress was concentrated at the exhaust edge of the listrium, the blade shroud near the inlet edge, and the middle of the blade shroud in the suction surface.

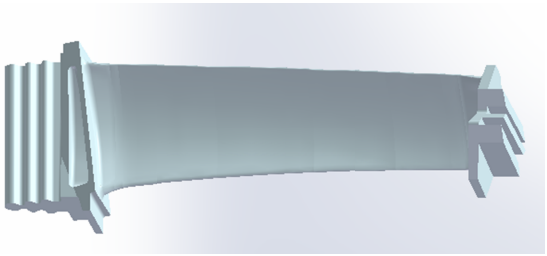

Fig. 12. Geometric model of gas turbine blades

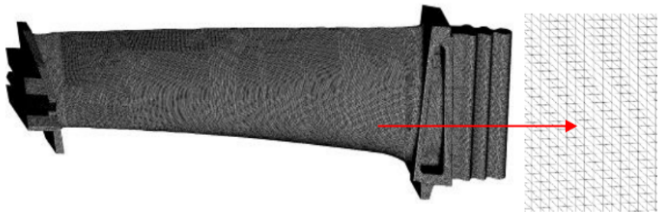

Fig. 13. Finite element model of the blade

The stress distribution of the blade body is illustrated in Fig. 15.

Fig. 15 shows that the stress concentration positions of the blade body were the exhaust edge of the listrium, the inlet edge near the blade shroud, and the inlet edge near the blade shroud of the suction surface

The areas of stress concentration, namely the assessment areas for strength, were marked as shown in Fig. 16. The stress distribution was analyzed based on the simulation values through analysis paths.

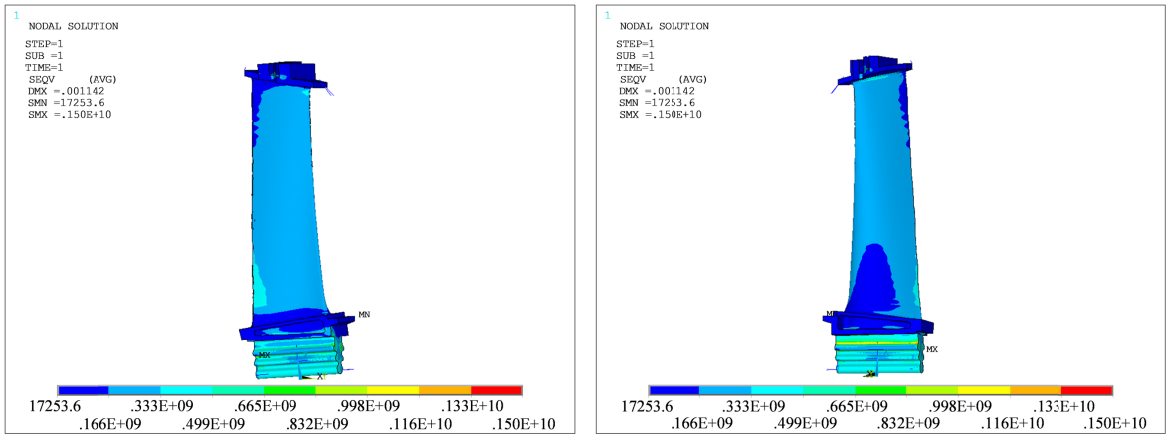

Fig. 14. Stress distribution of turbine blades

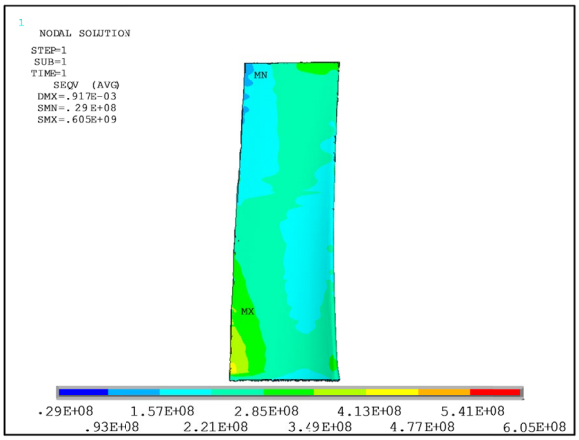

(a) Suction surface of the blade body

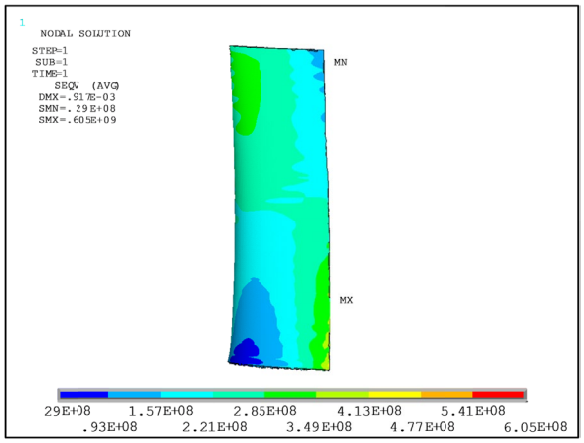

(b) Pressure surface of the blade body

Fig. 15. Stress distribution of the blade body

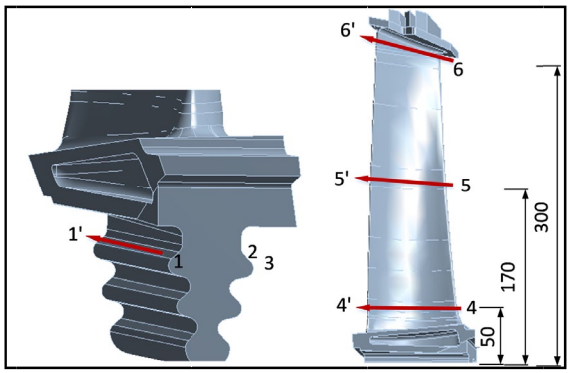

Fig. 16. Analysis paths of the tenon teeth and the blade body

Fig. 17 shows the stress distribution along paths 1-1', 2-2', and 3-3' at the blade tenon teeth.

Fig. 17 shows that the stress of the tenon 1, fillet 2 and tenon 3 at the inlet edge was relatively high. The stress of fillet 2 was the highest near the exhaust edge. The amplitude was close to 800 MPa.

Fig. 18 shows the stress distribution along paths 4-4' and 5-5' at the blade body.

Fig. 18 shows that the stress at the 4-4' position of the blade body was concentrated at the exhaust edge of the listrium. The maximum value was 332 MPa. The stress on the suction surface was greater than that on the pressure surface. The stress

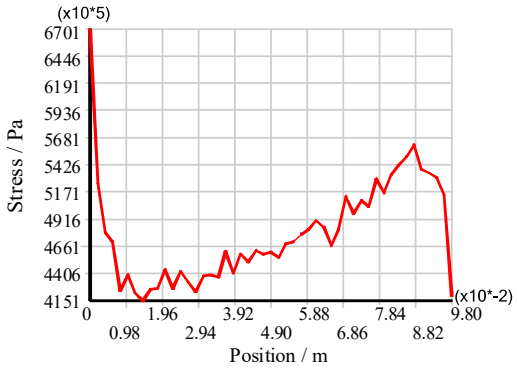

(a) 1-1' position

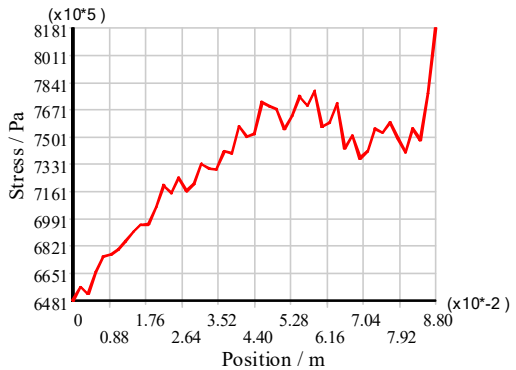

(b) 2-2'position

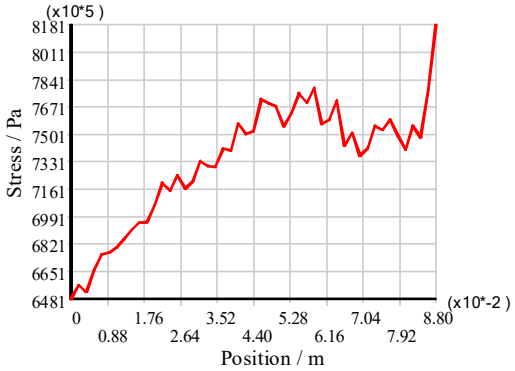

(c) 3-3' position

Fig. 17. Stress distribution along analysis paths of 1-1', 2-2', and 3-3'

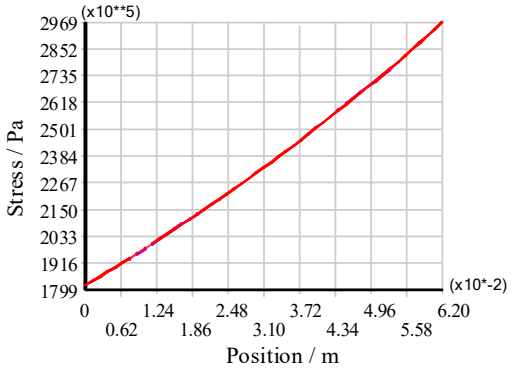

(a) 4-4' on the pressure surface

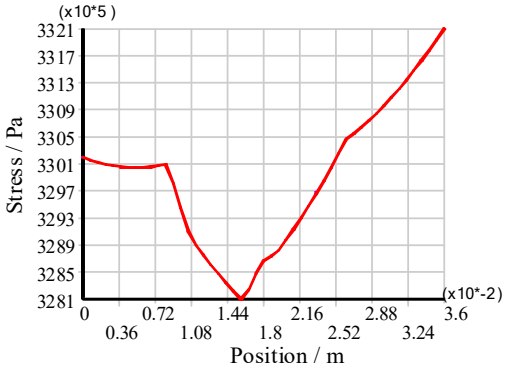

(b) 4-4' on the suction surface

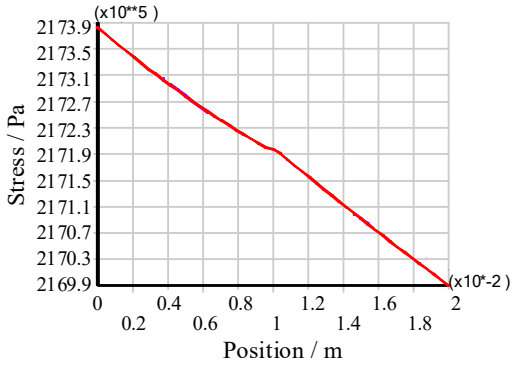

(c) 5-5' on the pressure surface

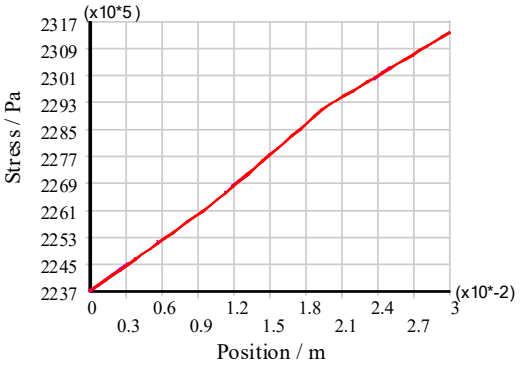

(d) 5-5' on the suction surface

Fig. 18. Stress distribution along analysis paths of 4-4' and 5-5'

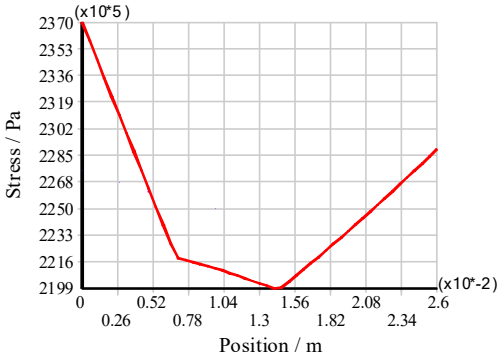

(a) 6-6' on the pressure surface

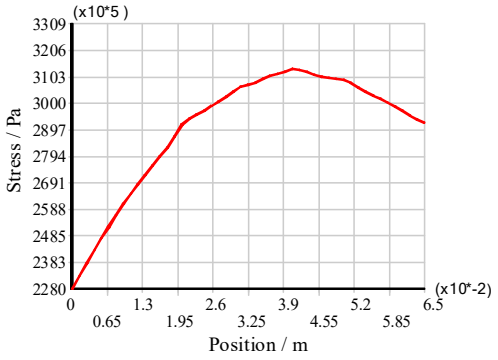

(b) 6-6' on the suction surface

Fig. 19. Stress distribution along analysis paths of 6-6’

distribution at the 5-5' position was relatively uniform. The stress amplitude was 210-240 MPa.

Fig. 19 shows the stress distribution along the path 6-6' near the blade shroud.

Fig. 19 shows that the stress on the inlet and the exhaust edges of the pressure surface at the 6-6' position was high. Stress values in the middle part of the suction surface were large, with the maximum value being 314 MPa. High-stress positions were located at the exhaust edges near the lower part of the blade body and the intake edge near the blade shroud.

The strength analysis for the turbine blade was carried out, and the stress distribution was obtained based on the mechanical property parameters of the MAR-M247 superalloy with heat treatment.

4. Conclusions

This study conducted a metallographic analysis of the MAR-M247 superalloy and a simulation analysis of the blade strength. The following conclusions were drawn from this study:

(1) Analysis of the results of metallographic experiments revealed that the heat treatment process influenced the grain size, phase γ', carbides, and eutectic phase γ/γ'. This indicated that the heat treatment improved the mechanical properties of the MAR-M247 superalloy.

(2) Based on the tensile tests, the mechanical properties of the MAR-M247 superalloy were calculated through material property simulation. The results provided the basis for the strength simulation analysis of the blade.

(3) The mechanical property parameters of the MAR-M247 superalloy were used in the strength simulation for the turbine blade. The finite element simulation analysis of the blade provided the stress distribution, and the strength of the turbine blade was evaluated. Accurate estimation of the strength of the turbine blades is significant.

Acknowledgments

This work was supported by the Fundamental Research Funds for the Central Universities (No: 2022JBZY028) and National Program on Key Basic Research Projects of China (No: 2013CB03570401).

REFERENCES

[1] L. Han, P. Li, S. Yu, et al., Creep/fatigue accelerated failure of Ni-based superalloy turbine blade: Microscopic characteristics and void migration mechanism. International Journal of Fatigue **154**, 106558 (2022). DOI: https://doi.org/10.1016/j.ijfatigue.2021.106558

[2] X. Li, W. Li, M. Lashari, et al., Fatigue failure behavior and strength prediction of nickel-based superalloy for turbine blade at elevated temperature. Engineering Failure Analysis **136**, 106191 (2022). DOI: https://doi.org/10.1016/j.engfailanal.2022.106191

[3] D. Ma, Novel casting processes for single-crystal turbine blades of superalloys. Frontiers of Mechanical Engineering **13** (1), 3-16 (2018). DOI: https://doi.org/10.1007/s11465-018-0475-0

[4] C. Zhang, P. Wang, Z. Wen, et al., Study on creep properties of nickel-based superalloy blades based on microstructure characteristics. Journal of Alloys and Compounds **890**, 161710 (2022). DOI: https://doi.org/10.1016/j.jallcom.2021.161710

[5] G. Salwan, R. Subbarao, S. Mondal, et al., Comparison and selection of suitable materials applicable for gas turbine blades. Materials Today: Proceedings **46** (17), 8864-8870 (2021). DOI: https://doi.org/10.1016/j.matpr.2021.05.003

[6] G. Erickson, The development and application of CMSX-10. Superalloys **1**, 35-44 (1996). DOI: https://doi.org/10.7449/1996/superalloys_1996_35_44

[7] R. Baldan, R. Rocha, R. Tomasiello, et al., Solutioning and aging of Mar-M247 nickel-based superalloy. Journal of Materials Engineering and Performance **22** (9), 2574-2579 (2017). DOI: https://doi.org/10.1007/s11665-016-2462-0

[8] N. Wan, M. Kang, N. Jung, et al., Failure analysis of the defect-induced blade damage of a compressor in the gas turbine of a co-generation plant. International Journal of Precision Engineering and Manufacturing **13** (5), 717-722 (2012). DOI: https://doi.org/10.1007/s12541-012-0093-4

[9] L. Sink, Development of low-cost directionally-solidified turbine blades, Mechanical Engineering (1980).

[10] L. Xing, L. Ke-An, T. Jia-Shi, et al., Analysis of Strength and Stiffness for Heavy-duty Gas Turbine Casing. Turbine Technology **53** (2), 85-88 (2011). DOI: https://doi.org/10.1016/j.matpr.2021.05.003

[11] G. Chen, J. Fan, S. Dong, et al., Strength uncertainty analysis of composite turbine blade with small sample size. Structures **6** (33), 1158-1179 (2021). DOI: https://doi.org/10.1016/j.istruc.2021.04.059

[12] H. Lin, H. Geng, X. Zhou, et al., High cycle fatigue analysis of third stage blade based on shroud gap effect. IEEE International Conference on Mechatronics and Automation **6**, 1781 (2016). DOI: https://doi.org/10.1109/ICMA.2016.7558834

[13] M. Reddy, P. Peyyala, S. Kaleru, et al., Analysis of gas turbine blade using finite element method. Proceedings of the 1st international conference on frontier of digital technology towards a sustainable society (2023). DOI: https://doi.org/10.1063/5.0116969.

[14] D. Boismier, A. Huseyin, ThermoMechanical Fatigue of Mar-M247: Part 1-Experiments. Journal of Engineering Materials & Technology **112** (1), 175-179 (1990). DOI: https://doi.org/10.1115/1.2903189

[15] G. Salwan, R. Subbarao, S. Mondal, Comparison and selection of suitable materials applicable for gas turbine blades. Materials Today: Proceedings **46** (17), 8864-8870 (2021). DOI: https://doi.org/10.1016/j.matpr.2021.05.003